Estimating the Power Capability of Li-ion Batteries Using Informationally Partitioned Estimators

Shankar Mohan, *Student Member, IEEE*, Youngki Kim, *Member, IEEE*, and Anna G. Stefanopoulou, *Fellow, IEEE*

***Abstract*— Enforcing constraints on the maximum deliverable power is essential to protect lithium-ion batteries and to maximize resource utilization. This paper describes an algorithm to address the estimation of power capability of battery systems accounting for thermal and electrical constraints. The algorithm is based on model inversion to compute the limiting currents and, hence, power capability. The adequacy of model inversion significantly depends on the accuracy of model states and parameters. Herein, these are estimated by designing cascading estimators whose structure is determined by quantifying the relative estimability of states and parameters. The parameterized battery model and the estimation algorithms are integrated with a power management system in a model of a series hybrid electric vehicle to demonstrate their effectiveness.**

***Index Terms*— Battery management, hybrid electric vehicle, lithium-ion (Li-ion) batteries, principal component analysis (PCA), state and parameter estimation.**

I. Introduction

LITHIUM-ION (Li-ion) batteries have high energy/power density and broad operating temperature ranges, making them ideal components of electrified vehicles [1], [2]. The performance and the longevity of these batteries hinge on constraining their operation, such that their terminal voltage, and internal and surface temperatures are regulated within prescribed ranges [3], [4]. With these batteries acting as power sources, an effective way to respect operating constraints is through the active regulation of powerflow—a task performed by a supervisory controller in electrified vehicles (refer to Fig. 1).

The power capability of a battery is the constant power that can be provided by or drawn over a finite window of time without violating operating constraints [5]. Methods to estimate power capability have been widely explored in the literature. Plett [5], Verbrugge and Koch [6], Anderson *et al.* [7], and Xiong *et al.* [8], using a representative equivalent-circuit model, computed the maximum admissible battery charge and discharge power ensuring that the battery's terminal voltage and State-of-Charge (SOC) remain constrained. Smith *et al.* [9] and Perez *et al.* [10] used a more physics-based electrochemical model to impose direct constraints on SOC and Li-ion concentration.

There is another constraint that significantly influences the rate of battery degradation of Li-ion batteries: temperature. It is well understood that operating batteries in elevated temperatures increases the potential for adverse side reactions and results in accelerated degradation [3]; however, it has not been factored-in when computing the power capability. This paper aims to address this lacuna by using reduced-order models to represent the electrical and thermal dynamics of the battery.

The electrical and thermal behaviors of Li-ion batteries depend on their current state and operating conditions. Since most power capability estimation techniques rely on model inversion, accurate information of the local dynamic behavior and estimates of internal states are desired. Thus, state–parameter estimation has been considered as an important aspect in the problem of power capability estimation [6]–[8], [11]. Broadly, the most common methods employed can be classified as being based on dual [11] or joint estimation [7], [8]. Dual estimation is often preferred, for it promises to minimize the influence of poor *a priori* knowledge of the values of parameters and poor quality of measurements on state estimates. In this paper, we propose another augmented-state–parameter-space (aSPs) partitioning technique based on a notion of relative estimability. A significance metric computed from a principal component analysis (PCA) on the Fisher information matrix (FIM), similar to the ones defined in [12]–[15] for offline parameter identification, is used to measure relative estimability. The aSPs is partitioned based on these significance metrics to aggregate elements, which have a similar influence on the system output. Finally, each partition is endowed with an estimator, in this instance an extended Kalman Filter (EKF).

The contribution of this paper is threefold as follows.

1) A simple and effective method to determine thermally and electrically constrained power capability of Li-ion batteries.
2) A quantitative metric—termed significance metric—is introduced to assess the estimability of states and parameters of the electrothermal battery model based on the FIM.
3) Partitioned estimators for online state–parameter identification are designed based on the significance metrics.

Manuscript received March 20, 2015; revised August 20, 2015; accepted November 5, 2015. Manuscript received in final form November 29, 2015. This work was supported by the Automotive Research Center through the U.S. Army Tank Automotive Research, Development and Engineering Center, Warren, MI, USA, under Grant W56HZV-04-2-0001. Recommended by Associate Editor S. Varigonda.

S. Mohan is with the Department of Electrical Engineering and Computer Science, University of Michigan, Ann Arbor, MI 48109 USA (e-mail: elemsn@umich.edu).

Y. Kim and A. G. Stefanopoulou are with the Department of Mechanical Engineering, University of Michigan, Ann Arbor, MI 48109 USA (e-mail: youngki@umich.edu; annastef@umich.edu).

Color versions of one or more of the figures in this paper are available online at http://ieeexplore.ieee.org.

Digital Object Identifier 10.1109/TCST.2015.2504847

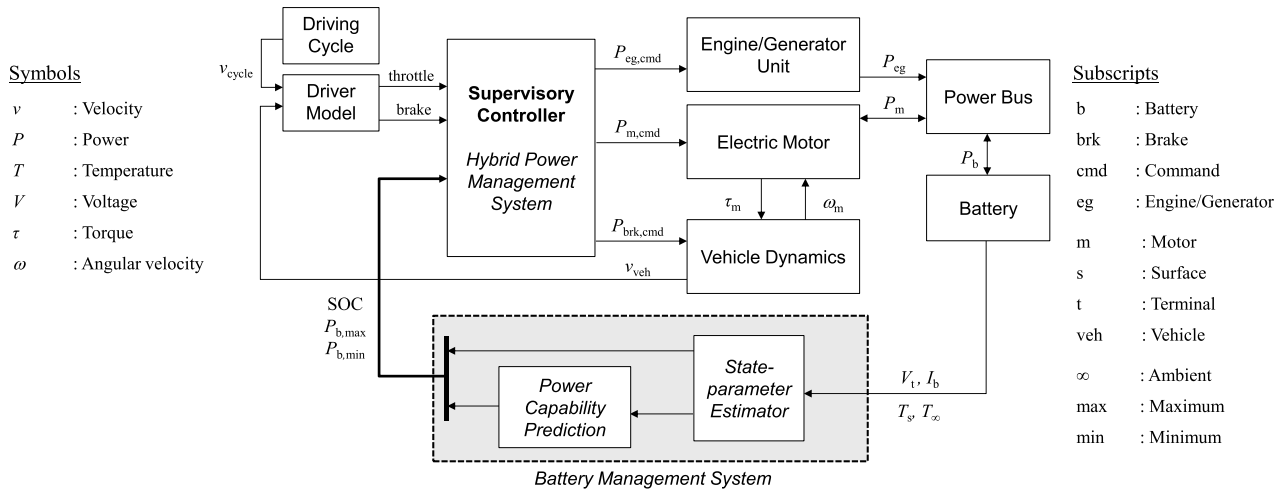

Fig. 1. Schematic of power and battery management systems in an SHEV simulation framework. The focus of this paper is on the battery management system (gray shaded box).

This paper is organized as follows. Section II describes the electrical and thermal dynamic models of the battery used in this paper. Section III details a method to estimate the power capability of a battery accounting for electrical and thermal constraints. Section IV proposes a quantitative metric based on the PCA to partition the augmented-state-space in designing estimators. Section V presents the control of a series hybrid electric vehicle (SHEV) as an example application of the presented techniques. Finally, Section VI concludes this paper with a summary of contributions and with a discussion on possible extensions.

II. Control-Oriented Battery Model

One of the objectives of this paper is to develop online estimation and control algorithms. To that end, simple control-oriented models are employed to capture the electrical and thermal behaviors of Li-ion batteries. In particular, an equivalent-circuit model for the electrical dynamics [16] and the reduced-order model developed in [17] for the thermal dynamics are adopted.

A. Electrical Dynamics

A two-state equivalent-circuit model is considered to predict terminal voltage, as shown in Fig. 2. The electrical dynamic behavior of the battery with the total capacity Q_b in discrete-time domain is described by

$$\begin{bmatrix} z_{k+1} \\ V_{1,k+1} \end{bmatrix} = \mathbf{A}_E \begin{bmatrix} z_k \\ V_{1,k} \end{bmatrix} + \mathbf{B}_E I_{b,k} \tag{1a}$$

$$V_{t,k} = V_{\text{oc}}(z_k) - V_{1,k} - R_{s,k} I_{b,k} \tag{1b}$$

where system matrices $\mathbf{A}_E$ and $\mathbf{B}_E$ are expressed by

$$\mathbf{A}_E = \begin{bmatrix} 1 & 0 \\ 0 & e^{\frac{-\Delta t}{R_{1,k} C_{1,k}}} \end{bmatrix}$$

$$\mathbf{B}_E = \begin{bmatrix} -\dfrac{\Delta t}{Q_b} \\ R_{1,k}\left(1 - e^{\frac{-\Delta t}{R_{1,k} C_{1,k}}}\right) \end{bmatrix}.$$

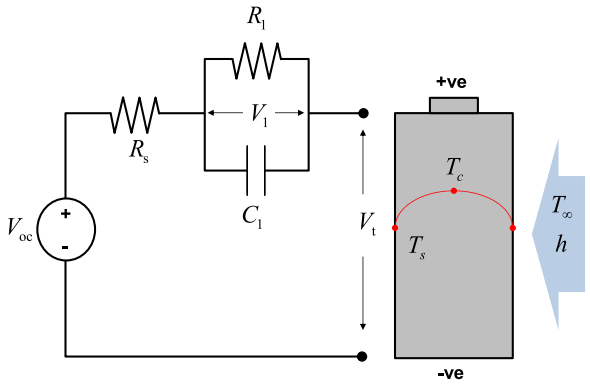

Fig. 2. Schematic of an electrothermal model for cylindrical batteries consisting of an equivalent-circuit model and 1-D thermal model.

The battery SOC, z, and polarization voltage, V_1, are states, i.e., $x_E = [z, V_1]'$, I_b is the current, and V_t and V_{oc} are the terminal voltage and open circuit voltage of the battery, respectively. The series resistance, R_s, and the polarization resistance/capacitance, (R_1, C_1), are the parameters to be estimated, i.e., $\theta_E = [R_s, R_1, C_1]'$. The subscript E denotes the electrical system to differentiate from the thermal system later. The sampling period in a battery management system is denoted by Δt. Refer to Appendix A for a list of nominal values of the parameters of the model when the cell under consideration is an A123 26650 LFP cell.

B. Thermal Dynamics

To predict core and surface temperatures of the battery, T_c and T_s, respectively, a reduced-order model developed in [17] is adopted and reproduced below for convenience

$$\begin{bmatrix} \bar{T}_{k+1} \\ \bar{y}_{k+1} \end{bmatrix} = \mathbf{A}_T \begin{bmatrix} \bar{T}_k \\ \bar{y}_k \end{bmatrix} + \mathbf{B}_T \begin{bmatrix} \dot{q}_k \\ T_{\infty,k} \end{bmatrix} \tag{2a}$$

$$\begin{bmatrix} T_{c,k} \\ T_{s,k} \end{bmatrix} = \mathbf{C}_T \begin{bmatrix} \bar{T}_k \\ \bar{y}_k \end{bmatrix} + \mathbf{D}_\mathbf{T} T_{\infty,k} \tag{2b}$$

where $\bar{T}$ is the averaged temperature and $\bar{\gamma}$ is the averaged temperature gradient. The above model was derived from the simple 1-D heat equation assuming uniform heat generation across the radius of the cylindrical cell and a quadratic form for the temperature distribution along the radial direction. Ambient temperature and the rate of heat generation are denoted by T_∞ and $\dot{q}$, respectively. The subscript T denotes the thermal system. Matrices of the thermal system are given by

$$\mathbf{A}_T = \begin{bmatrix} \dfrac{hr^2+24k_tr-48\alpha h\Delta t}{r(24k_t+rh)} & \dfrac{-15\alpha h\Delta t}{24k_t+rh} \\ \dfrac{-320\alpha h\Delta t}{r^2(24k_t+rh)} & \dfrac{hr^3+24k_tr^2-120\alpha\Delta t(rh+4k_t)}{r^2(24k_t+rh)} \end{bmatrix}$$

$$\mathbf{B}_T \triangleq [\mathbf{B}_{T_1} \quad \mathbf{B}_{T_2}] = \begin{bmatrix} \dfrac{\alpha\Delta t}{k_tV_b} & \dfrac{48\alpha h\Delta t}{r(24k_t+rh)} \\ 0 & \dfrac{320\alpha h\Delta t}{r^2(24k_t+rh)} \end{bmatrix}$$

$$\mathbf{C}_T \triangleq \begin{bmatrix} \mathbf{C}_{T_1} \\ \mathbf{C}_{T_2} \end{bmatrix} = \begin{bmatrix} \dfrac{24k_t-3rh}{24k_t+rh} & -\dfrac{120rk_t+15r^2h}{8(24k_t+rh)} \\ \dfrac{24k_t}{24k_t+rh} & \dfrac{15rk_t}{48k_t+2rh} \end{bmatrix}$$

$$\mathbf{D}_T \triangleq \begin{bmatrix} \mathbf{D}_{T_1} \\ \mathbf{D}_{T_2} \end{bmatrix} = \begin{bmatrix} \dfrac{4rh}{24k_t+rh} \\ \dfrac{rh}{24k_t+rh} \end{bmatrix}$$

where r, k_t, and α are the radius, thermal conductivity, and thermal diffusivity of the battery, respectively; typically, these parameters are not significantly affected by operating temperature. However, the convection coefficient, h, is highly influenced by cooling or heating condition, and hence, it is chosen to be a parameter to be estimated. States and parameters of the thermal dynamics for the online estimation are $x_T = [\bar{T}, \bar{\gamma}]'$ and $\theta_T = h$, respectively. Refer to Appendix VI for a list of nominal values of the parameters of the model when the cell under consideration is an A123 26650 LFP cell.

The heat generation rate, $\dot{q}$, is determined by the electrical dynamics as

$$\dot{q}_k = I_{b,k}^2 R_{s,k} + \frac{V_{1,k}^2}{R_{1,k}} - I_{b,k}\bar{T}_k\frac{\Delta S_k}{F} \tag{3}$$

where F is Faraday's constant, 96 485.3365 C/mol; ΔS denotes the entropy change of the battery and is related to a certain amount of energy that needs to be reversibly absorbed or released to balance the whole reaction inside the battery.

III. Power Capability Estimation

In determining power capability, the following factors are considered.

1) The thermal and electrical dynamics of a Li-ion battery are intrinsically coupled.
2) The internal resistance and the rate of change of internal resistance with respect to temperature decrease with increasing temperature.
3) For a galvanostatic operation, any arbitrary increase in battery temperature causes reduced internal losses, and subsequently generates less heat.
4) Over a short time horizon, changes in temperature and SOC are assumed to be bounded.

The above statements are valid insofar as the battery temperature does not exceed the threshold temperature at which thermal runaway is initiated. Since thermal dynamics are much slower than electrical dynamics, in determining the power capability, the thermal and electrical constraint problems are addressed separately.

To calculate the power capability of the battery, an algebraic propagation (AP) method is applied with information about states and parameters from the state–parameter estimators developed in Section IV. The AP method computes a constant input, which leads to that none of constraints are violated in N future steps. To apply the AP method to the electrical system, the output of system (1) needs to be linearized and is expressed as

$$\begin{bmatrix} z_{k+1} \\ V_{1,k+1} \end{bmatrix} = \mathbf{A}_E(R_{1,k}, C_{1,k})\begin{bmatrix} z_k \\ V_{1,k} \end{bmatrix} + \mathbf{B}_E(R_{1,k}, C_{1,k})I_{b,k} \tag{4a}$$

$$\begin{bmatrix} z_k \\ V_{t,k} \end{bmatrix} = \mathbf{C}_E\begin{bmatrix} z_k \\ V_{1,k} \end{bmatrix} + \mathbf{D}_E I_{b,k} + \mathbf{E}_E \tag{4b}$$

where matrices $\mathbf{C}_E$, D_E, and $\mathbf{E}_E$ are defined as

$$\mathbf{C}_E \triangleq \begin{bmatrix} \mathbf{C}_{E_1} \\ \mathbf{C}_{E_2} \end{bmatrix} = \begin{bmatrix} 1 & 0 \\ \left.\dfrac{\partial V_{\rm oc}(z)}{\partial z}\right|_{z=z_k} & -1 \end{bmatrix}$$

$$\mathbf{D}_E \triangleq \begin{bmatrix} \mathbf{D}_{E_1} \\ \mathbf{D}_{E_2} \end{bmatrix} = \begin{bmatrix} 0 \\ -R_{s,k} \end{bmatrix}$$

$$\mathbf{E}_E \triangleq \begin{bmatrix} \mathbf{E}_{E_1} \\ \mathbf{E}_{E_2} \end{bmatrix} = \begin{bmatrix} 0 \\ V_{\rm oc}(z_k) - \left.\dfrac{\partial V_{\rm oc}(z)}{\partial z}\right|_{z=z_k} z_k \end{bmatrix}.$$

The maximum permissible currents accounting for electrical constraints, such as SOC and voltage limits, $\mathrm{SOC}_{\min}$, $\mathrm{SOC}_{\max}$, $V_{\min}$, and $V_{\max}$, are determined, respectively, as in (5a)–(5d), as shown at the bottom of the next page. Each of those equations, in sequence, helps compute the value of constant current that will drive SOC to lower limit, SOC to upper limit, terminal voltage to lower limit, and terminal voltage to upper limit, at the end of an N-step prediction window. The derivation of each subequation in (5) follows the same steps; thus, for simplicity, the derivation of (5a) is provided in the following. At any instant k, the N-step ahead prediction of the various states assuming a constant current, I_b, is given by

$$\begin{bmatrix} z_{k+N} \\ V_{1,k+N} \end{bmatrix} = \mathbf{A}_E^N\begin{bmatrix} z_k \\ V_{1,k} \end{bmatrix} + \left(\sum_{i=1}^{N-1}\mathbf{A}_E^i\mathbf{B}_E\right)I_b. \tag{6}$$

If the value of SOC at the end of N samples is equal to $\mathrm{SOC}_{\min}$, then the value of continuous discharge charge current ($I_{b,\max,k}^{\mathrm{SOC}_{\min}}$) that drives the SOC to lower boundary is computed by enforcing the terminal constraint on (6)

$$\mathrm{SOC}_{\min} = \mathbf{C}_{E_1}\begin{bmatrix} z_{k+N} \\ V_{1,k+N} \end{bmatrix} + I_{b,\max,k}^{\mathrm{SOC}_{\min}}\mathbf{D}_{E_1} + \mathbf{E}_{E_1}.$$

Now, substituting (6) into the above and collecting terms, (5a) is derived.

For the battery thermal system, the representation in (2) is rewritten as the following equations:

$$\begin{bmatrix}\bar{T}_{k+1}\\ \gamma_{k+1}\end{bmatrix} = \mathbf{A}_T(h_k)\begin{bmatrix}\bar{T}_k\\ \gamma_k\end{bmatrix} + \mathbf{B}_{T_1}(h_k)\mu_k + \xi_{1,k} \tag{7a}$$

$$T_{c,k} = \mathbf{C}_{T_1}(h_k)\begin{bmatrix}\bar{T}_k\\ \gamma_k\end{bmatrix} + \xi_{2,k} \tag{7b}$$

where

$$\mu_k = I_{b,k}^2 R_{s,k} - I_{b,k}\bar{T}_k\frac{\Delta S_k}{F} \tag{8a}$$

$$\xi_{1,k} = \mathbf{B}_{T_1}(h_k)\begin{bmatrix}V_{1,k}^2\\ R_{1,k}\\ T_{\infty,k}\end{bmatrix} \tag{8b}$$

$$\xi_{2,k} = D_{T_1}(h_k)T_{\infty,k}. \tag{8c}$$

When the prediction period is short, the battery SOC and the temperature do not change significantly over the prediction horizon. Thus, it is reasonable to assume that the entropy change and the internal resistance are constant over the prediction horizon, i.e., $R_{s,j|k} \approx R_{s,k}$ and $\Delta S_{j|k} \approx \Delta S_k$ for $j = k, k+1, \ldots, k+N$. In addition, the ambient temperature and the convection coefficient do not change rapidly and, hence, are assumed to be constant, i.e., $T_{\infty,j|k} \approx T_{\infty,k}$ and $h_{j|k} \approx h_k$ for $j = k, k+1, \ldots, k+N$. Finally, an estimate of heat generation by the polarization voltage over the prediction horizon is obtained through model iteration using the maximum permissible current at the previous sampling time

$$\bar{\xi}_{1,k} = \max\{\xi_{1,k}, \xi_{1,k+N}\}. \tag{9}$$

These approximations make it easy to handle the nonlinearity in the expression of a heat generation rate using a quadratic term $I_{b,k}^2$ and a bilinear term $I_{b,k}\bar{T}_k$.

Then, the maximum of the input $\mu_{\max,k}^q$, $q \in \{\text{dch}, \text{chg}\}$, which is described by considering the maximum core temperature $T_{c,\max}$, is determined as in (10a) and (10b), as shown at the bottom of this page. Superscripts dch and chg represent battery discharge and charge, respectively. By substituting (10) into (8a), the maximum permissible currents during battery discharge and charge are determined, respectively, by the following equations:

$$I_{b,\max,k}^{T_{\max}} = \frac{\frac{\bar{T}_k\Delta S_k}{F} + \sqrt{\left(\frac{\bar{T}_k\Delta S_k}{F}\right)^2 + 4R_{s,k}\mu_{\max,k}^{\text{dch}}}}{2R_{s,k}} \tag{11a}$$

$$I_{b,\min,k}^{T_{\max}} = \frac{\frac{\bar{T}_k\Delta S_k}{F} - \sqrt{\left(\frac{\bar{T}_k\Delta S_k}{F}\right)^2 + 4R_{s,k}\mu_{\max,k}^{\text{chg}}}}{2R_{s,k}}. \tag{11b}$$

Maximum discharge and charge currents accounting for all constraints are calculated with

$$I_{b,\max,k} = \min\left\{I_{b,\max,k}^{\text{SOC}_{\min}}, I_{b,\max,k}^{V_{\min}}, I_{b,\max,k}^{T_{\max}}\right\} \tag{12a}$$

$$I_{b,\min,k} = \max\left\{I_{b,\min,k}^{\text{SOC}_{\max}}, I_{b,\min,k}^{V_{\max}}, I_{b,\min,k}^{T_{\max}}\right\}. \tag{12b}$$

Finally, the power capability $\{P_{b,\max,k}, P_{b,\min,k}\}$ is computed by the product of the maximum allowable current and terminal voltage after N future sample steps expressed as

$$P_{b,\max,k} = I_{b,\max,k}\cdot V_{t,k+N|k}^{\text{dch}} \tag{13a}$$

$$P_{b,\min,k} = I_{b,\min,k}\cdot V_{t,k+N|k}^{\text{chg}} \tag{13b}$$

$$I_{b,\max,k}^{\text{SOC}_{\min}} = \left(\sum_{i=0}^{N-1}\mathbf{C}_{E_1}\mathbf{A}_E^i\mathbf{B}_E + \mathbf{D}_{E_1}\right)^{-1}\left(\text{SOC}_{\min} - \mathbf{C}_{E_1}\mathbf{A}_E^N\begin{bmatrix}z_k\\ V_{1,k}\end{bmatrix} - \mathbf{E}_{E_1}\right) \tag{5a}$$

$$I_{b,\min,k}^{\text{SOC}_{\max}} = \left(\sum_{i=0}^{N-1}\mathbf{C}_{E_1}\mathbf{A}_E^i\mathbf{B}_E + \mathbf{D}_{E_1}\right)^{-1}\left(\text{SOC}_{\max} - \mathbf{C}_{E_1}\mathbf{A}_E^N\begin{bmatrix}z_k\\ V_{1,k}\end{bmatrix} - \mathbf{E}_{E_1}\right) \tag{5b}$$

$$I_{b,\max,k}^{V_{\min}} = \left(\sum_{i=0}^{N-1}\mathbf{C}_{E_2}\mathbf{A}_E^i\mathbf{B}_E + \mathbf{D}_{E_2}\right)^{-1}\left(V_{\min} - \mathbf{C}_{E_2}\mathbf{A}_E^N\begin{bmatrix}z_k\\ V_{1,k}\end{bmatrix} - \mathbf{E}_{E_2}\right) \tag{5c}$$

$$I_{b,\min,k}^{V_{\max}} = \left(\sum_{i=0}^{N-1}\mathbf{C}_{E_2}\mathbf{A}_E^i\mathbf{B}_E + \mathbf{D}_{E_2}\right)^{-1}\left(V_{\max} - \mathbf{C}_{E_2}\mathbf{A}_E^N\begin{bmatrix}z_k\\ V_{1,k}\end{bmatrix} - \mathbf{E}_{E_2}\right) \tag{5d}$$

$$\mu_{\max,k}^{\text{dch}} = \left(\sum_{i=0}^{N-1}\mathbf{C}_T\mathbf{A}_T^i\mathbf{B}_T\right)^{-1}\left(T_{c,\max} - \mathbf{C}_T\mathbf{A}_T^N\begin{bmatrix}\bar{T}_k\\ \gamma_k\end{bmatrix} - \sum_{i=0}^{N-1}\mathbf{C}_T\mathbf{A}_T^i\bar{\xi}_{1,k}^{\text{dch}} - \xi_{2,k}\right) \tag{10a}$$

$$\mu_{\max,k}^{\text{chg}} = \left(\sum_{i=0}^{N-1}\mathbf{C}_T\mathbf{A}_T^i\mathbf{B}_T\right)^{-1}\left(T_{c,\max} - \mathbf{C}_T\mathbf{A}_T^N\begin{bmatrix}\bar{T}_k\\ \gamma_k\end{bmatrix} - \sum_{i=0}^{N-1}\mathbf{C}_T\mathbf{A}_T^i\bar{\xi}_{1,k}^{\text{chg}} - \xi_{2,k}\right) \tag{10b}$$

where the predicted terminal voltage $V^q_{k+N|k}$, $q \in \{\text{dch}, \text{chg}\}$ is calculated with

$$V^{\text{dch}}_{t,k+N|k} = V_{\text{oc}}\left(z_k - \frac{I_{b,\max,k} N \Delta t}{Q_b}\right) - I_{b,\max,k} R_{s,k} - e^{\frac{-N\Delta t}{R_{1,k}C_{1,k}}} V_{1,k} - I_{b,\max,k} R_{1,k}\left(1 - e^{\frac{-N\Delta t}{R_{1,k}C_{1,k}}}\right)$$

$$V^{\text{chg}}_{t,k+N|k} = V_{\text{oc}}\left(z_k - \frac{I_{b,\min,k} N \Delta t}{Q_b}\right) - I_{b,\min,k} R_{s,k} - e^{\frac{-N\Delta t}{R_{1,k}C_{1,k}}} V_{1,k} - I_{b,\min,k} R_{1,k}\left(1 - e^{\frac{-N\Delta t}{R_{1,k}C_{1,k}}}\right).$$

IV. State and Parameter Estimation

The power capability of a battery, as described in Section III, relies on the accurate description of the battery's electrothermal dynamics. The challenge of estimating model states and parameters in the context of power capability estimation has been extensively studied; broadly, the most common methods employed can be classified as being based on dual [11] or joint estimation [7], [8].

In this section, the problem of state–parameter estimation is addressed by describing a method to partition the aSPs for dual estimation. The partitioning is inspired by spectral techniques that have, thus, far been used for offline parameterization of models, and the resulting partitions are worked upon by a cascading estimator. To that end, this section is structured as follows. Section IV-A describes the partitioning technique in general. Section IV-B specializes the method to the problem of state–parameter estimation for the electrothermal model and describes the overall structure of the estimator.

A. Partitioning of the Augmented-State-Space

Joint estimation in the aSPs is generally computationally intensive and is less preferred to dual estimation, because the latter is believed to reduce the influence of poor *a priori* knowledge of initial parameters and poor measurements on state estimates [11], [18], [19]. In a typical implementation of a dual estimator, the aSPs is partitioned into two groups consisting of states and parameters, respectively. In this paper, based on the notion of observability/estimability, an alternate criterion to partition the aSPs is suggested. The proposed partitioning technique is a direct extension of standard offline parameter estimation techniques [12], [20].

Consider a general dynamic system whose evolution is described by the following equations:

$$x_{k+1} = f(x_k, \theta_k, u_k) \tag{14a}$$

$$y_k = g(x_k, \theta_k, u_k) \tag{14b}$$

where $f, g \in \mathcal{C}^1(\mathbb{R}^{n_x} \times \mathbb{R}^{n_p} \times \mathbb{R}^{n_u})$. Suppose it is of interest to estimate the states, x, and the parameters, θ, in the presence of exogenous inputs, u; the aSPs description for the estimator is defined as follows:

$$\tilde{x}_{k+1} = f(\tilde{x}_k, u_k) \tag{15a}$$

$$y_k = g(\tilde{x}_k, u_k) \tag{15b}$$

where $\tilde{x} = [x, \theta]' \in \mathbb{R}^{n_x+n_p}$. The parameters, θ, are assumed time-invariant or slow-varying, over a short window of data of length N samples. State–parameter estimation problems can generally be recast as one of finding the initial condition of states and parameters in the form of a least squares estimation (LSE) problem [21]

$$\tilde{\theta} = \arg\min_{\tilde{\theta}} \ \|Y - \hat{Y}(\tilde{\theta}, U)\|^2 \tag{16}$$

where $\tilde{\theta} = [x_0, \theta]'$; x_0 is the initial condition of states, θ is the parameter of the dynamical system, U is the vector of inputs $U = [u_1, \ldots, u_N]'$, Y is the vector of measurements $Y = [y_1, \ldots, y_N]'$, and $\hat{Y}$ is the output of the model $\hat{Y}(\tilde{\theta}) = [\hat{y}_1(\tilde{\theta}), \ldots, \hat{y}_N(\tilde{\theta})]'$. In the following discussion, the FIM is used as a tool to asses the estimability of parameters $\tilde{\theta}$.[1]

The FIM, $\mathbf{F}$, is typically constructed by stacking a sequence of sensitivity coefficients. In the context of the LSE problem in (16), $\mathbf{F} = \mathbf{H}'\mathbf{H}$ where

$$\mathbf{H}(\hat{\tilde{\theta}}, Y, U) = [\text{diag}(Y)]^{-1} \left[\begin{array}{ccc} \frac{\partial y_1(\tilde{\theta}, U)}{\partial \tilde{\theta}_1} & \cdots & \frac{\partial y_1(\tilde{\theta}, U)}{\partial \tilde{\theta}_{n_x+n_p}} \\ \vdots & \ddots & \vdots \\ \frac{\partial y_N(\tilde{\theta}, U)}{\partial \tilde{\theta}_1} & \cdots & \frac{\partial y_N(\tilde{\theta}, U)}{\partial \tilde{\theta}_{n_x+n_p}} \end{array}\right]\Bigg|_{\tilde{\theta}=\hat{\tilde{\theta}}} \times [\ \text{diag}(\hat{\tilde{\theta}})] \tag{17}$$

$\hat{\tilde{\theta}}$ is the best *a priori* estimate of $\tilde{\theta}$, and it has been assumed that measurement uncertainty, if any, is additive white Gaussian with unit variance. Observe that the Jacobian is left multiplied by a diagonal matrix of measurements from the model, and is multiplied from the right by a diagonal matrix of the values of the various parameters. The Jacobian matrix is thus scaled to normalize entries and remove any units associated with entries.[2]

The FIM provides useful information about the estimation problem—the rank of $\mathbf{F}$ presents the number of estimable parameters, an ill-conditioned $\mathbf{F}$ indicates that some parameters are not robustly estimable, the inverse of $\mathbf{F}$ is termed the covariance matrix and is related to the variance of estimates as derived by the best unbiased estimator (the Cramér–Rao bound). The information matrix has been used for yet another purpose—to infer the relative significance of estimating parameters from the provided data. This form of analysis, typically reserved for offline parameterization, has been discussed in the literature (refer to [12]–[15] and references therein); studies on offline estimability typically culminate in a method to partition the set of parameters to be estimated, $\tilde{\theta}$, into groups. Herein, a similar partitioning technique is utilized to design the online estimator.

A quantitative metric to assist in ranking parameters based on their relative significance on the measurement and, hence, their estimability from the measurement can be defined using PCA [20], [23] on FIM. In the following discussion, for

[1] For the relation between FIM and local nonlinear observability, refer to [22].

[2] Viewed differently, one could say that the various parameters—each a random variable—are scaled to create new random variables and the Jacobian is with respect to the new random variables.

Algorithm 1 Cascading Estimation Algorithm (SISO)

Data: Y, U and $\tilde{\theta}_{k-1}$
Initialize $\tilde{\theta}_k$;
Build G_1 and G_2;
Set $i = 1$;
while $i \leq 2$ **do**
  val$(G_i) = \psi_i(G_1, G_2, Y, U)$;
  $i = i + 1$;
end
Update θ_k from G_1 and G_2.
where ψ_i is an estimator designed for group G_i.

Algorithm 2 Ranking States/Parameters

Data: Current, output and state trajectories associated with a drive-cycle
Result: $\bar{\eta}$, the average significance vector,
Let X be the *states* of interest;
Set $L :=$ length of drive-cycle;
Set $n_{\tilde{\theta}} = \dim(\theta)$;
Set $n_h := 2n_{\tilde{\theta}} + 1$;
Set $i = 1$;
while $i \leq L - n_h + 1$ **do**
  $\mathbf{H} = \mathbf{H}(X(i), Y_i^{i+n_h-1}, U_i^{n_h-1})$;
  $\mathbf{F} = \mathbf{H}'\mathbf{H}$;
  $\forall j \in \mathbb{N} \cap [1, n_\theta]$, $\boldsymbol{\Upsilon}_{i,j} = \eta_j$;
end
$\bar{\eta} := \bar{\boldsymbol{\Upsilon}}'$;
where $\bar{\boldsymbol{\Upsilon}}$ is the row average of the columns of $\boldsymbol{\Upsilon}$ and Y_i^{i+a} represents a vector consisting of elements i through $i + a$ of Y.

simplicity of expressions, it is assumed that the $\mathbf{F}$ has distinct eigenvalues. Let $r = n_x + n_p$ and $\Lambda = \{\lambda_1, \ldots, \lambda_r\}$ be the ordered set (increasing) of eigenvalues of the $\mathbf{F}$, and $\{E_1, \ldots, E_r\}$ be the set of eigenvectors arranged to match the corresponding eigenvalue. The principal components of $\mathbf{H}$ and the eigenvectors of $\mathbf{F}$ are ordered as follows—$\forall i, j \in \mathbb{N}_r$, if $i < j$, E_j explains the variation in the data better than E_i. The relative significance of principal components is a reflection of the corresponding directions along which there is a larger variation. A measure of the significance of the ith parameter, $\tilde{\theta}_i$, is given by

$$\eta_i = \frac{\sum_{k=1}^{r} |\lambda_k \cdot (E_k)_i|}{\sum_{k=1}^{r} |\lambda_k|} \tag{18}$$

where $(E_k)_i$ denotes the ith row of E_k. Note that $0 \leq \eta_i \leq 1$ and reflects the difficulty of estimating the ith parameter by itself; if $\eta_i > \eta_j$, the ith parameter is more estimable than the jth parameter. Let Θ be the set of all the elements of the aSP that are to be estimated, and ζ is the critical threshold about which the parameters are partitioned. For notational convenience, it is assumed that $\zeta \in [0, 1]$. Then, two vectorized groups G_1 and G_2 can be defined as follows:

$$G_1 = \text{vec}(\{\tilde{\theta}_i \in \Theta \mid \zeta \leq \eta_i \leq 1\}) \tag{19a}$$

$$G_2 = \text{vec}(\Theta \backslash \{\tilde{\theta}_i \in \Theta \mid \zeta \leq \eta_i \leq 1\}) \tag{19b}$$

The online estimation problem at every update instant k is depicted in Algorithm 1. At each update instance, estimates of the value taken by elements in the aSP are updated in a sequence with groups consisting of more significant elements being updated earlier than groups with less significant elements. In Algorithm 1, $\tilde{\theta}_{k-1}$ is the estimate of every element of aSP using the information available until instance $k-1$; *a priori* estimates of $\tilde{\theta}_k$ are derived from $\tilde{\theta}_{k-1}$ using the dynamics in (15). This is followed by initializing the values of elements in G_j using the *a priori* estimates of $\tilde{\theta}_k$. The value of members of each group is subsequently updated using measurement information of inputs and outputs (U and Y) and *a priori* estimates; this is achieved using estimator ψ_i associated with group G_i. The ψ_is in the algorithm are estimators designed specific to group G_is and are chosen, such that the extent to which measurements influence the updates decreases as the group number increases. At each instant k, as such, the following equality holds:

$$e_k^2 \leq e_k^1$$

where e_k^1 is the output prediction error having updated G_1 and G_2 is the total output prediction error after all states and parameters have been updated. The availability of individually tunable parameters for each group is an additional degree of freedom that the designer can utilize to address the problem that typically attributed to joint estimation; by detuning the estimators associated with G_2, the impact of measurement noise on the less observable states/parameters can be reduced.

Remark 1: As elements in each group have comparable influence on the measured output, in our experience, tuning individual estimators is simpler than when the cascading structure was not adopted.

B. State–Parameter Estimation of the Electrothermal Model

Section IV-A presented the architecture of the estimator considered in this paper—the aSPs was partitioned based on metrics derived from the FIM of the initial condition estimation problem. This section addresses the problem of state–parameter estimation of the electrothermal model.

Fundamental to the application of the cascading algorithm in Algorithm 1 is the availability of the significance metric η. In offline parameterization problems, the entire trajectory of the inputs and outputs is completely known, and the ranking algorithm can be set up as described in Section IV-A; however, for online estimation problems, particularly for nonlinear estimation, when the employed estimator works with a limited data set, the parameter significance ranking has to be performed dynamically using a window of data. However, since a Battery Management System (BMS) platform, in general, does not have sufficient computational power, the expected influence of parameters is computed offline by generating a meaningful set of data as described.

The average significance of each element in the aSPs over which the estimator operates is computed by utilizing standard drive cycles. For each drive cycle, the model of the integrated SHEV presented in [24] is used to generate the trajectory of

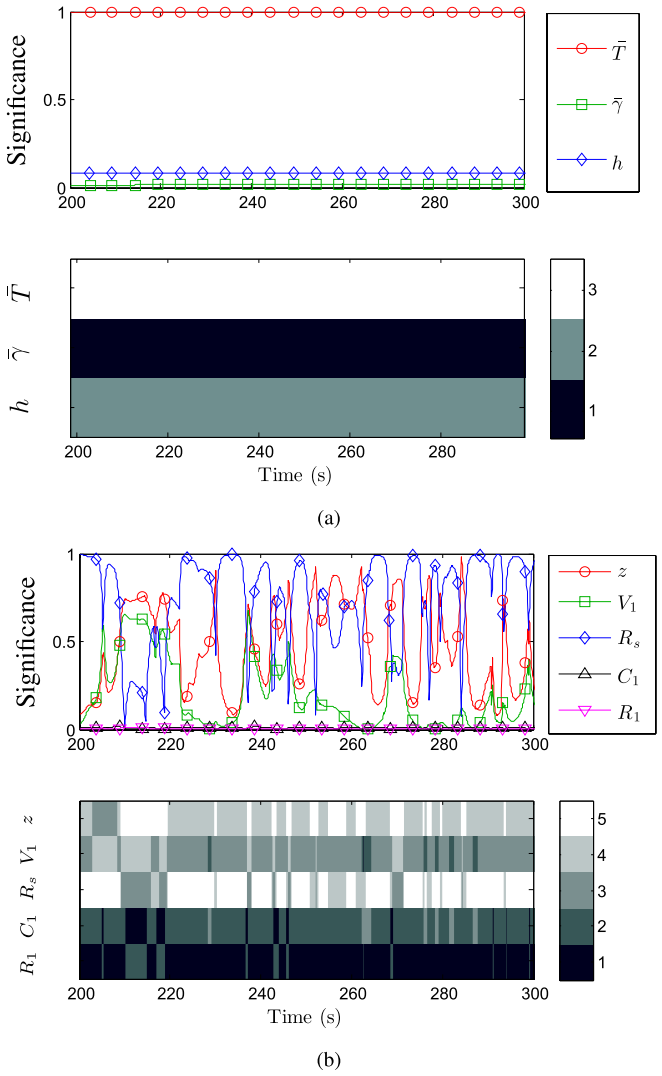

Fig. 3. Tracing the significance of each state/parameter in the (a) thermal aSP while measuring surface temperature alone (b) electrical aSP when measuring terminal voltage, along the UAC drive-cycle.

battery currents. The generated current profile is, in turn, fed to the battery pack model, and the resulting output voltage and the trajectories of the internal states and parameters are recorded similar to [25]. Considering the minimum number of samples required to estimate n parameters from data, $2n+1$, as suggested in [26], the information matrix is computed along the trajectory of the states, and the associated significance of each element of aSPs is computed, as described in Algorithm 2. The significance metrics, computed at each instance based on a receding history, are then averaged to compute the significance metric over the entire drive cycle.

Fig. 3(a) and (b) presents the evolution of the significance metric associated with each element of the aSPs, for both the thermal and electrical subsystems. The metrics are evaluated over a rolling data set obtained from driving the heavy-duty vehicle model to follow the urban assault cycle (UAC) [24]. The first subplot of both figures traces the values of the significance metrics, while the second subplot provides an indication of the relative ranking of the significance metrics at every time instant; it should be noted that in the second plot, higher the relative rank, the more significant the parameter.

From Fig. 3(a), it is observed that the average temperature gradient, $\bar{\gamma}$, has the least influence on the surface temperature T_s. The surface temperature is structurally more influenced by the averaged temperature than by the thermal gradient as can be observed from system matrix C_{T_2} (2). In addition, the influence of perturbation of h on the surface temperature is dominated by the ratio of thermal conductivity to radius; that is, when the battery with low thermal conductivity has small radius, it is expected that a change in convection coefficient does not lead to any discernable change in the surface temperature.

Unlike Fig. 3(a), Fig. 3(b) exhibits a slightly erratic pattern; however, the key traits are fairly predictable. As the influence of the parameters of the single R–C pair manifests themselves through the trajectory of the polarization voltage, it is expected that these parameters are not any more estimable than V_1. The contribution of V_1 to the terminal voltage is usually smaller than that of the series resistance and the open-circuit voltage in terms of magnitude. This behavior arises from the current in hybrid vehicles being typically charge sustaining. Thus, on an average, R_s—the most significant parameter to compute the power capability [27]—is the most estimable parameter and the average significance metric mirrors our expectations of estimability of states and parameters. Note that when the current is identically zero, the series resistance is not estimable; in producing Fig. 3, it was assumed that the pack is always excited with some current.

Remark 2: It is worth reiterating that the aSP of the electrical and thermal models of the battery is, in this paper, partitioned based on average significance metrics. This choice was made by observing that the relative ranking of the various states/parameters—computed using Algorithm 2—remains fairly constant. This is to be expected when the battery operates at or above room temperature, and in an HEV application, wherein the SOC deviates about a nominal (not by much). However, for a generic nonlinear system, if the solution trajectory was such that the local behavior at any two instances was sufficiently different, then the number of partitions and their members will have to be dynamically adjusted.

Remark 3: The parameters of the equivalent-circuit model that are considered for online estimation has one glaring omission—battery capacity; an accurate estimate of the cell's capacity is assumed. The cell's measurable capacity is a function of temperature and the magnitude of power fed/drawn; an inaccurate estimate constitutes a structural uncertainty in the dynamics of the electrical subsystem. A discussion on the impact of this uncertainty on the quality of estimates and the structure of the estimator is deferred until a subsequent work.

V. Power Management in a Hybrid Electric Vehicle

This section investigates the performance of the proposed power capability estimator and its influence on the power management in a heavy-duty SHEV. The SHEV is simulated in the cosimulation framework in which the battery electrothermal model and the online adaptive estimators are fully integrated to the vehicle model.

TABLE I
SIGNIFICANCE OF STATES AND PARAMETER TO OUTPUTS OVER DIFFERENT INPUT PROFILES BASED ON PCA

Cycle	Electrical					Thermal		
	$\bar{\eta}_z$	$\bar{\eta}_{V_1}$	$\bar{\eta}_{R_s}$	$\bar{\eta}_{C_1}$	$\bar{\eta}_{R_1}$	$\bar{\eta}_{\bar{T}}$	$\bar{\eta}_{\bar{\gamma}}$	$\bar{\eta}_h$
UAC	0.485	0.170	0.682	0.008	0.002	0.996	0.027	0.078
ECC	0.455	0.189	0.560	0.007	0.002	0.996	0.016	0.081
HD-UDDS	0.364	0.199	0.456	0.005	0.003	0.996	0.016	0.081

$\bar{\eta}_*$ is the average significance metric corresponding to state/parameter $*$, over the entire drive-cycle. Refer to Section II for a list of all parameters.

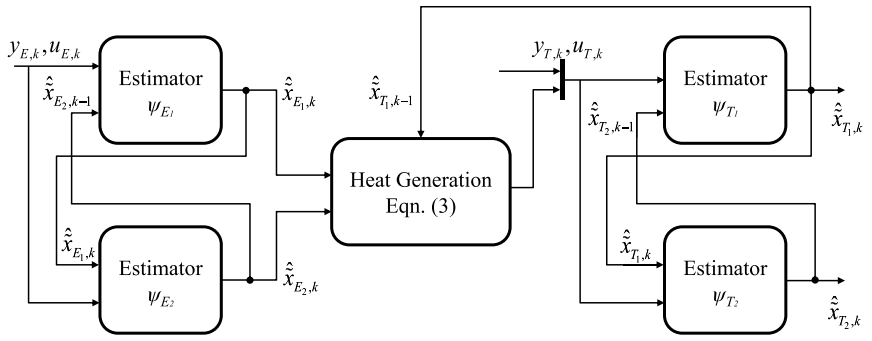

Fig. 4. Schematic of state–parameter estimators with cascading structure.

The HEV simulator is developed using a forward-looking approach, as shown in Fig. 1. The driver, which takes the desired and actual vehicle velocities as inputs and provides propulsion or braking power demands, is modeled as a PI controller. Powertrain components, such as the engine/generator, motor, and battery, are modeled with quasi-static maps.

In the simulator, power distribution is managed using a receding horizon controller whose instantaneous objective is to optimally minimize a weighted cost function: fuel consumption, SOC deviation, and power rate of the engine/generator. Details of the controller and its implementation are not of immediate relevance to the contents of this paper and, hence, have not been included; they can be found in [24].

Extending the presentation in Section IV, Algorithm 2 is iterated over three different standard heavy-duty vehicles' drive cycles. Table I tabulates the computed expected relative influence for the thermal and electrical subsystems over these drive cycles. The mean significance of each state/parameter $*$ is denoted by $\bar{\eta}_*$. From a cursory glance at the numerical estimates of expected significance, one notes a self-evident partitioning of the aSPs, and Table II collates the relevant groups for both subsystems [using $\zeta = 0.1$ in (19) for both the electrical and thermal subsystems]. With these partitions, independent estimators are designed for each group, as shown in Fig. 4. Note that the states/parameters of the electrical systems are estimated solely based on terminal voltage, but those of the thermal systems are influenced by estimates of the electrical systems through (3). To reflect this dependence, estimates of the electrical subsystem are updated prior to those of the thermal subsystem. The estimator of choice is the EKF summarized briefly in Appendix B.

TABLE II
STATE, PARAMETER, INPUT, AND OUTPUT OF ELECTRICAL AND THERMAL SYSTEMS FOR STATE–PARAMETER ESTIMATION

	Electrical	Thermal
G_1	$\tilde{x}_{E_1,k} = [z_k,\, V_{1,k},\, R_{\mathrm{s},k}]'$	$\tilde{x}_{T_1,k} = \bar{T}_k$
G_2	$\tilde{x}_{E_2,k} = [R_{1,k},\, C_{1,k}]'$	$\tilde{x}_{T_2,k} = [\bar{\gamma}_k,\, h_k]'$
Input	$u_{E,k} = I_{\mathrm{b},k}$	$u_{T,k} = [\dot{q}_k,\, T_{\infty,k}]'$
Output	$y_{E,k} = V_{\mathrm{t},k}$	$y_{T,k} = T_{\mathrm{s},k}$

A. Estimator Tuning

The average significance metric, as presented in Section IV, enables one to determine quantitatively the relative extent to which variation in the measured data can be explained by each element of the augmented-state-space. Viewed differently, the inverse of the significance metric is roughly indicative of the relative variance of the estimates of the states and parameters obtained from the provided data; the EKFs used in this paper are tuned with this information. Matrices **Q** and **R**, which correspond to the process and measurement noise covariance matrices, respectively, are set as follows.

Recall that the average significance metric of parameter $*$, $\bar{\eta}_*$, was computed from the eigenvalues of the FIM and that the FIM matrix was computed from the scaled Jacobian. Scaling the Jacobian can be interpreted as scaling the parameters. To compute the expected variance of each parameter, the inverse of the significance metric has to be multiplied by the square of the scaling factor—the nominal value of the parameter.

TABLE III
NOMINAL VALUES AND DERIVATIVE MATRICES

Parameter	z	V_1	R_s	C_1	R_1	$\bar{T}$	$\bar{\gamma}$	h
Value	0.5	0.1	10^{-3}	1.5×10^{3}	10^{-3}	30	30	15

$$\begin{aligned}
\mathbf{N}_{E_1} &= \text{diag}([z_{\text{nom}}^2, V_{1\text{nom}}^2, R_{s\text{nom}}^2]) \\
\mathbf{N}_{E_2} &= \text{diag}([C_{1\text{nom}}^2, R_{1\text{nom}}^2]) \\
\mathbf{N}_{T_1} &= \text{diag}([\bar{T}_{\text{nom}}^2]) \\
\mathbf{N}_{T_2} &= \text{diag}([\bar{\gamma}_{\text{nom}}^2, h_{\text{nom}}^2])
\end{aligned}$$

Thus, the $\mathbf{Q}$ matrix for every estimator employed is defined as follows:

$$\begin{aligned}
\mathbf{Q}_{E_1} &= \text{diag}([1/\bar{\eta}_z, 1/\bar{\eta}_{V_1}, 1/\bar{\eta}_{R_s}]) \cdot \mathbf{N}_{E_1} \\
\mathbf{Q}_{E_2} &= \text{diag}([1/\bar{\eta}_{C_1}, 1/\bar{\eta}_{R_1}]) \cdot \mathbf{N}_{E_2} \\
\mathbf{Q}_{T_1} &= \text{diag}([1/\bar{\eta}_{\bar{T}}]) \cdot \mathbf{N}_{T_1} \\
\mathbf{Q}_{T_2} &= \text{diag}([1/\bar{\eta}_{\bar{\gamma}}, 1/\bar{\eta}_h]) \cdot \mathbf{N}_{T_2}
\end{aligned}$$

where $\bar{\eta}_*$ is the mean significance metric of state $*$ presented in Table I and the matrix on the right of each expression, $\mathbf{N}$, is a diagonal matrix comprised of the square of the nominal value of the corresponding parameter $*_{\text{nom}}$. Table III collates the nominal values of various parameters and the derived nominal matrices.

The values of $\bar{\eta}_*$'s are computed from the scaled version of the Jacobian, $\mathbf{H}$ [refer to (17)].[3] The listed $\mathbf{Q}$ matrices correspond to the electrical (subscript E) and thermal (subscript T) subsystems, respectively, and the numeral subscript corresponds to the group number. With the $\mathbf{Q}$ matrices defined as above, the values of the corresponding $\mathbf{R}$ matrices are tuned to minimize the mean error in individual estimates of states and parameters. The matrix $\mathbf{R}$ is tuned by scaling appropriately sized identity matrices, and the mean error threshold is chosen to be 5%. In this particular application, the values of the corresponding $\mathbf{R}$ matrices are the following:

$$\begin{aligned}
\mathbf{R}_{E_1} &= 10^4, \quad \mathbf{R}_{E_2} = 10^4 \\
\mathbf{R}_{T_1} &= 10^{-4}, \quad \mathbf{R}_{T_2} = 10^3.
\end{aligned}$$

B. Results and Discussion

The battery current and the terminal voltage, which are inputs to the EKF-based estimator for the electrical system $\psi_{E.}$, are shown in Fig. 5. To simulate realistic noise conditions, the current and the voltage are contaminated with artificial Gaussian noises, i.e., $\sigma_I = 3 \times 10^{-3}$ and $\sigma_V = 1 \times 10^{-3}$. The results of state–parameter estimation for the electrical system are shown in Fig. 6(a)–(e), indicating that the estimator $\psi_{E.}$ can simultaneously estimate SOC,[4] polarization voltage, series resistance, polarization resistance, and capacitance. It is observed that states and parameters

[3]When a random variable is scaled, its variance is also quadratically scaled; the right diagonal matrices for $\mathbf{Q}$ are in place to normalize the entries of the corresponding states.

[4]The battery SOC from the plant model is measured using Coulomb counting.

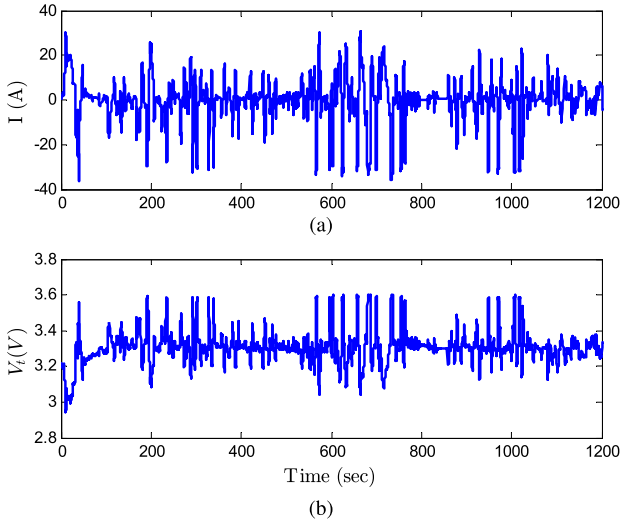

Fig. 5. Input data to the estimators $\psi_{E.}$ over the UAC. (a) Current. (b) Terminal voltage.

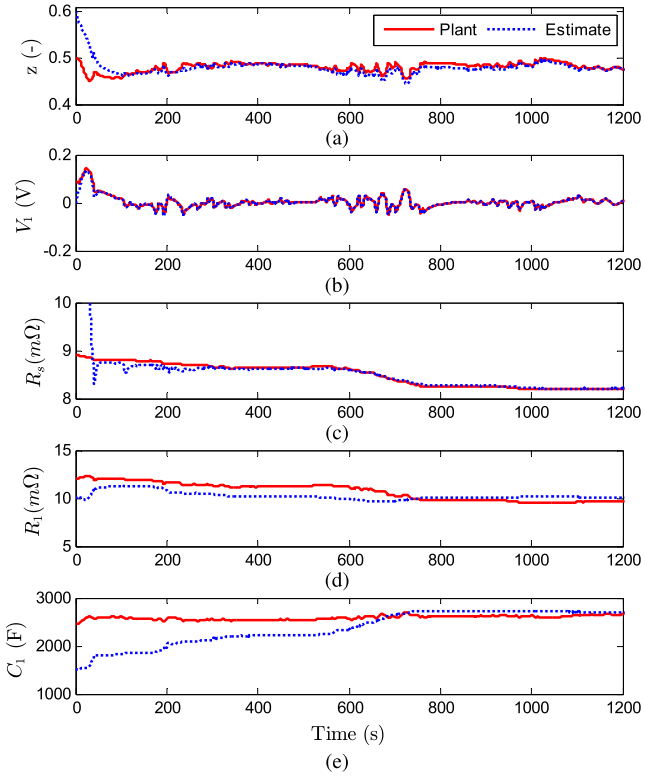

Fig. 6. Performance of the estimator for the electrical system $\psi_{E.}$ (a) SOC. (b) Polarization voltage. (c) Series resistance. (d) Polarization resistance. (e) Polarization capacitance.

in G_1 are estimated accurately and their convergence rates are relatively fast compared with those in G_2. In particular, polarization resistance R_1 has the lowest estimation quality, which corresponds to the result that R_1 has the smallest significance metric among states and parameters.

Fig. 7 shows the battery surface temperature and the ambient temperature, which are used as inputs to the EKF-based estimator for the thermal system $\psi_{T.}$; similar to electrical system, Gaussian noises are artificially added to the surface and ambient temperatures, i.e., $\sigma_{T_s} = \sigma_{T_\infty} = 1.57 \times 10^{-3}$.

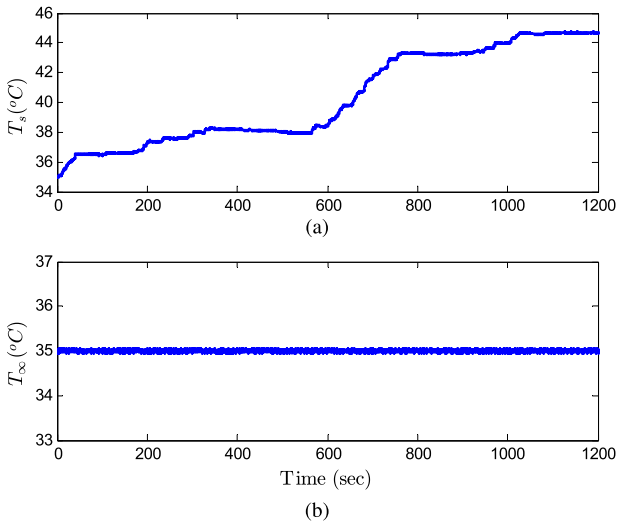

Fig. 7. Input data to the estimator ψ_T over the UAC. (a) Surface temperature. (b) Ambient temperature.

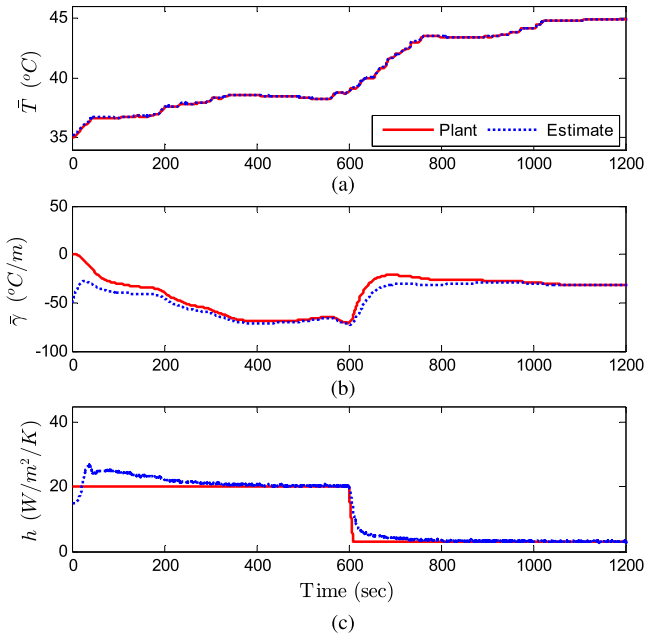

Fig. 8. Performance of the estimator for the thermal system ψ_T. (a) Averaged temperature. (b) Averaged thermal gradient. (c) Convection coefficient.

To simulate malfunction of the cooling system, the convection coefficient is deliberately changed from 20 to 3 W/m^2-K at $t = 600$ s. This malfunction condition is simulated to assess not only the performance of the estimator ψ_T, but also the effectiveness of the power capability estimation. As shown in Fig. 8, the estimator is capable of providing accurate estimates of the states and parameters of the thermal system.

Remark 4: The controller employed by the simulator aims to minimize fuel consumption while also regulating battery SOC; the objective function of the controller is formulated as the weighted sum of fuel consumption and SOC deviation about 0.5. Since the optimization problem is solved in receding horizon fashion without any terminal or invariant set constraints, the SOC at the end of the simulation should

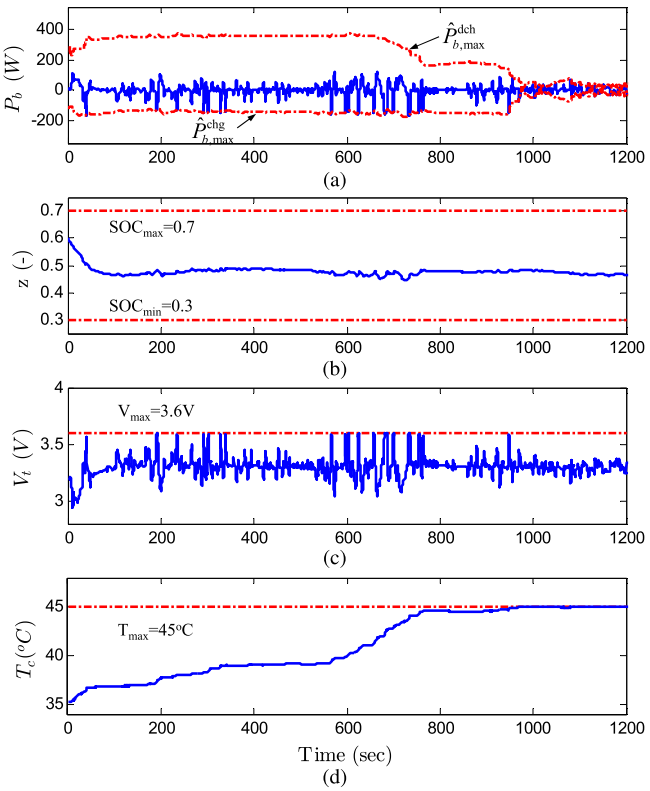

Fig. 9. Performance of the power capability estimation. (a) Power. (b) SOC. (c) Terminal voltage. (d) Core temperature.

not be expected to be identical to 0.5 despite the general formulation being labeled charge sustaining. In addition, if the thermal constraints are active, then the power that can be drawn and or deposited into the pack decreases, making SOC regulation more challenging.

The results of power capability estimation are shown in Figs. 9 and 10, which depict the battery power, SOC, terminal voltage, and core temperature. Each subplot has the trajectory of the variable in blue line and the bounds on its value in red line. As shown in Fig. 9(a), the maximum battery power is limited by electrical-constrained power capability when the battery core temperature is lower than the target value of $T_{c,\max} = 45$ °C. It is observed that the battery SOC and the terminal voltage do not violate constraints [Fig. 9(b) and (c)]. However, as the core temperature increases, thermal-constrained power capability becomes active, and hence, the battery power is effectively regulated between the maximum and minimum power limits. To highlight this performance, specific time periods from 1000 to 1100 s are shown in Fig. 10. Consequently, the core temperature is well regulated around the maximum temperature, as shown in Fig. 10(d); $\max\{\hat{T}_c - T_c, 0\} = 0.02$. Considering that the accuracy of a thermocouple is usually less than 0.5 °C and that the convection coefficient h is estimated from noisy measurements, it can be said that the performance of the proposed method is reasonably satisfactory.

Evidenced by the results from the model-in-the-loop simulation, it can be concluded that the developed estimation algorithms, including states, parameters, and power capabil-

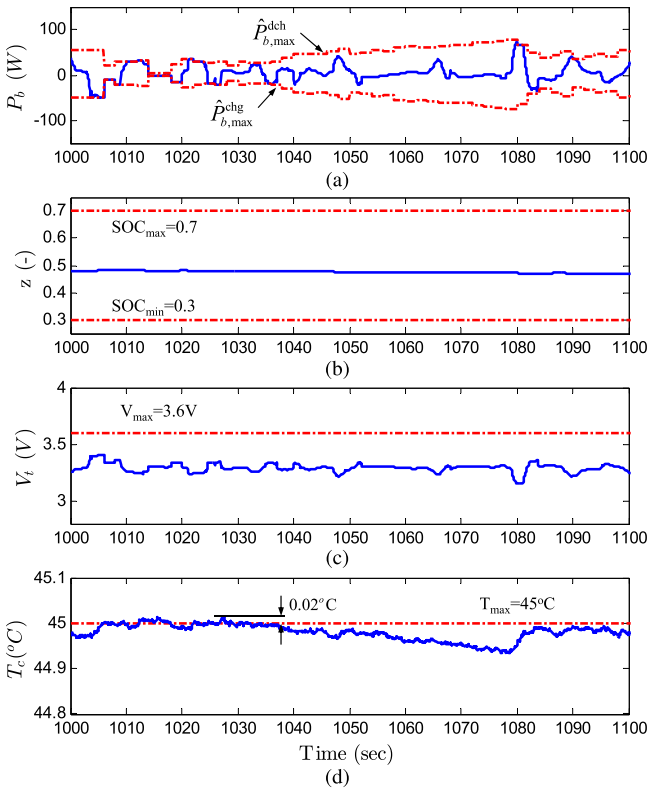

Fig. 10. Performance of the power capability estimation from 1000 to 1100 s. (a) Power. (b) SOC. (c) Terminal voltage. (d) Core temperature.

ity, are capable of providing accurate information about the battery. Thus, the safe and reliable operation of the power management system as well as the battery can be achieved.

VI. Conclusion

This paper presents a method to estimate the thermally and electrically constrained power capability of battery systems and demonstrates its application to the power management problem in an SHEV. The dynamics of the electrical and thermal subsystems are not invariant and, hence, are adapted. To design estimators/adaptors, the relative estimability of the states and parameters of the electrical and thermal models was studied using the PCA. Based on a ranking table derived from their relative estimability, the elements of the augmented-state-space model were grouped based on an average significance metric, and individual estimators were designed for each group. The results of the model-in-the-loop simulation show that the proposed estimation algorithms can provide accurate information about the battery to the power management system, and hence, safe and reliable operation of the SHEV can be achieved. A future work will explore the possibility of allowing for dynamically altering the number of groups and their membership based on the local significance of the various states and parameters.

Appendix A
List of Parameters of the Model

This section lists the nominal values of the parameters in the models introduced in Section II when the pack under consideration consists of A123 26650 LFP cells.

Parameter	Symbol	Value
Density	ρ	2047
Sp. heat coeff.	c_p	1109.2
Thermal cond.	k_t	0.610
Conv. coeff.	h	58.6
Series Resistance	R_s	0.0106
Polarization resistance	R_1	0.0169
Polarization capacitance	C_1	2249
Cell capacity	Q_b	2.3

Appendix B
Overview of the Extended Kalman Filter

A brief summary of the EKF methodology used in Section V is provided in this appendix.

Considering a dynamical system described by

$$\begin{aligned} \tilde{x}_{k+1} &= f(\tilde{x}_k, u_k) + v_k \\ y_k &= g(\tilde{x}_k, u_k) + w_k \end{aligned}$$

with the process and measurement noises, v_k and w_k, respectively, define the following:

$$\mathbf{A}_{k-1} = \left.\frac{\partial f}{\partial \tilde{x}}\right|_{\left\{\begin{array}{l}\tilde{x}=\hat{\tilde{x}}^+_{k-1}\\ u=u_{k-1}\end{array}\right\}}, \quad \mathbf{C}_k = \left.\frac{dg}{d\tilde{x}}\right|_{\left\{\begin{array}{l}\tilde{x}=\hat{\tilde{x}}^-_{k}\\ u=u_{k}\end{array}\right\}}.$$

The design of each EKF estimator is given as the following update processes assuming that the covariances of the process and measurements noises are defined as $\mathbf{Q} := E\{v'_k v_k\}$ and $\mathbf{R} := E\{w'_k w_k\}$, respectively.

Time Update for the State Filter:

$$\begin{aligned} \hat{\tilde{x}}^-_k &= \mathbf{A}_{k-1}\hat{\tilde{x}}^+_{k-1} + \mathbf{B}_{k-1}u_{k-1} \\ \mathbf{P}^-_k &= \mathbf{A}_{k-1}\mathbf{P}^+_{k-1}\mathbf{A}^T_{k-1} + \mathbf{Q}. \end{aligned}$$

Measurement Update for the State Filter:

$$\begin{aligned} \mathbf{K}_k &= \mathbf{P}^-_k \mathbf{C}_k{}^T \left[\mathbf{C}_k \mathbf{P}^-_k \mathbf{C}_k{}^T + \mathbf{R}\right]^{-1} \\ \hat{\tilde{x}}^+_k &= \hat{\tilde{x}}^-_k + \mathbf{K}_k\left[y_k - f_{u_k}\left(\hat{\tilde{x}}^-_k\right)\right] \\ \mathbf{P}^+_k &= [\mathbf{I} - \mathbf{K}_k\mathbf{C}_k]\mathbf{P}^-_k. \end{aligned}$$

References

[1] R. Huggins, *Advanced Batteries: Materials Science Aspects*. Springer, 2008. [Online]. Available: http://dx.doi.org/10.1007/978-0-387-76424-5.

[2] Z. Rao and S. Wang, "A review of power battery thermal energy management," *Renew. Sustain. Energy Rev.*, vol. 15, no. 9, pp. 4554–4571, 2011.

[3] J. Shim, R. Kostecki, T. Richardson, X. Song, and K. A. Striebel, "Electrochemical analysis for cycle performance and capacity fading of a lithium-ion battery cycled at elevated temperature," *J. Power Sour.*, vol. 112, no. 1, pp. 222–230, 2002.

[4] R. Spotnitz and J. Franklin, "Abuse behavior of high-power, lithium-ion cells," *J. Power Sour.*, vol. 113, no. 1, pp. 81–100, 2003.

[5] G. L. Plett, "High-performance battery-pack power estimation using a dynamic cell model," *IEEE Trans. Veh. Technol.*, vol. 53, no. 5, pp. 1586–1593, Sep. 2004.

[6] M. Verbrugge and B. Koch, "Generalized recursive algorithm for adaptive multiparameter regression application to lead acid, nickel metal hydride, and lithium-ion batteries," *J. Electrochem. Soc.*, vol. 153, no. 1, pp. A187–A201, 2006.

[7] R. D. Anderson, Y. Zhao, X. Wang, X. G. Yang, and Y. Li, "Real time battery power capability estimation," in *Proc. Amer. Control Conf.*, Jun. 2012, pp. 592–597.
[8] R. Xiong, H. He, F. Sun, X. Liu, and Z. Liu, "Model-based state of charge and peak power capability joint estimation of lithium-ion battery in plug-in hybrid electric vehicles," *J. Power Sour.*, vol. 229, pp. 159–169, May 2013.
[9] K. A. Smith, C. D. Rahn, and C.-Y. Wang, "Model-based electrochemical estimation and constraint management for pulse operation of lithium ion batteries," *IEEE Trans. Control Syst. Technol.*, vol. 18, no. 3, pp. 654–663, May 2010.
[10] H. Perez, N. Shahmohammadhamedani, and S. Moura, "Enhanced performance of li-ion batteries via modified reference governors and electrochemical models," *IEEE/ASME Trans. Mechatronics*, vol. 20, no. 4, pp. 1511–1520, Aug. 2015.
[11] G. L. Plett, "Extended Kalman filtering for battery management systems of LiPB-based HEV battery packs: Part 3. State and parameter estimation," *J. Power Sour.*, vol. 134, no. 2, pp. 277–292, 2004.
[12] K. Schittkowski, "Experimental design tools for ordinary and algebraic differential equations," *Ind. Eng. Chem. Res.*, vol. 46, no. 26, pp. 9137–9147, 2007.
[13] B. R. Jayasankar, A. Ben-Zvi, and B. Huang, "Identifiability and estimability study for a dynamic solid oxide fuel cell model," *Comput. Chem. Eng.*, vol. 33, no. 2, pp. 484–492, 2009.
[14] A. P. Schmidt, M. Bitzer, Á. W. Imre, and L. Guzzella, "Experiment-driven electrochemical modeling and systematic parameterization for a lithium-ion battery cell," *J. Power Sour.*, vol. 195, no. 15, pp. 5071–5080, 2010.
[15] J. C. Forman, S. J. Moura, J. L. Stein, and H. K. Fathy, "Genetic identification and fisher identifiability analysis of the Doyle–Fuller–Newman model from experimental cycling of a $LiFePO_4$ cell," *J. Power Sour.*, vol. 210, pp. 263–275, Jul. 2012.
[16] X. Hu, S. Li, and H. Peng, "A comparative study of equivalent circuit models for Li-ion batteries," *J. Power Sour.*, vol. 198, pp. 359–367, Jan. 2012.
[17] Y. Kim, S. Mohan, J. B. Siegel, A. G. Stefanopoulou, and Y. Ding, "The estimation of temperature distribution in cylindrical battery cells under unknown cooling conditions," *IEEE Trans. Control Syst. Technol.*, vol. 22, no. 6, pp. 2277–2286, Nov. 2014.
[18] E. A. Wan and A. T. Nelson, "Dual Kalman filtering methods for nonlinear prediction, smoothing, and estimation," in *Proc. Adv. Neural Inf. Process. Syst. 9*, pp. 793–799, 1997.
[19] M. C. VanDyke, J. L. Schwartz, and C. D. Hall, "Unscented Kalman filtering for spacecraft attitude state and parameter estimation," in *Proc. 14th AAS/AIAA Space Flight Mech. Conf.*, Feb. 2004, pp. 217–228.
[20] R. Li, M. A. Henson, and M. J. Kurtz, "Selection of model parameters for off-line parameter estimation," *IEEE Trans. Control Syst. Technol.*, vol. 12, no. 3, pp. 402–412, May 2004.
[21] P. E. Moraal and J. W. Grizzle, "Observer design for nonlinear systems with discrete-time measurements," *IEEE Trans. Autom. Control*, vol. 40, no. 3, pp. 395–404, Mar. 1995.
[22] C. Jauffret, "Observability and fisher information matrix in nonlinear regression," *IEEE Trans. Aerosp. Electron. Syst.*, vol. 43, no. 2, pp. 756–759, Apr. 2007.
[23] G. H. Dunteman, *Principal Components Analysis*. Newbury Park, CA, USA: Sage, 1989, vol. 69.
[24] Y. Kim, A. Salvi, A. G. Stefanopoulou, and T. Ersal, "Reducing soot emissions in a diesel series hybrid electric vehicle using a power rate constraint map," *IEEE Trans. Veh. Technol.*, vol. 64, no. 1, pp. 2–12, Jan. 2015.
[25] X. Lin *et al.*, "A lumped-parameter electro-thermal model for cylindrical batteries," *J. Power Sour.*, vol. 257, pp. 1–11, Jul. 2014.
[26] D. Aeyels, "On the number of samples necessary to achieve observability," *Syst. Control Lett.*, vol. 1, no. 2, pp. 92–94, Aug. 1981.
[27] X. Hu, R. Xiong, and B. Egardt, "Model-based dynamic power assessment of lithium-ion batteries considering different operating conditions," *IEEE Trans. Ind. Informat.*, vol. 10, no. 3, pp. 1948–1959, Aug. 2014.

Shankar Mohan (S'11) received the bachelor's degree in electrical engineering from the National University of Singapore, Singapore, in 2011, and the master's degree in electrical engineering from the University of Michigan, Ann Arbor, MI, USA, in 2013, where he is currently pursuing the Ph.D. degree in electrical engineering.

His current research interests include numerical optimization methods and the application of control techniques to energy systems.

Youngki Kim (M'14) received the B.S. and M.S. degrees from the School of Mechanical and Aerospace Engineering, Seoul National University, Seoul, Korea, in 2001 and 2003, respectively, and the Ph.D. degree from the Mechanical Engineering Department, University of Michigan, Ann Arbor, MI, USA, in 2014.

He was a Research Engineer with the Research and Development Division, Hyundai Motor Company, Seoul, from 2003 to 2008. He is currently a Post-Doctoral Research Fellow with the Powertrain Control Laboratory, University of Michigan. His current research interests include modeling, simulation, and optimal control/estimation of dynamic systems, such as electrified vehicles and electrochemical energy storage systems.

Anna G. Stefanopoulou (F'09) was an Assistant Professor with the University of California at Santa Barbara, Santa Barbara, CA, USA, from 1998 to 2000, and a Technical Specialist with Ford Motor Company, Dearborn, MI, USA, from 1996 to 1997. She is currently a Professor of Mechanical Engineering with the University of Michigan, Ann Arbor, MI, USA, and the Director of the Automotive Research Center, a university-based U.S. Army Center of Excellence in Modeling and Simulation of Ground Vehicles.

Dr. Stefanopoulou is a fellow of the American Society of Mechanical Engineers (ASME), the Founding Chair of the ASME DSCD Energy Systems Technical Committee, and a member of a U.S. National Academies Committee on U.S. Vehicle Fuel Economy Standards. She has co-authored a book on Control of Fuel Cell Power Systems, 14 U.S. patents, five best paper awards, and 250 publications on estimation and control of internal combustion engines and electrochemical processes, such as fuel cells and batteries.